The Synthesis and Structure of SSZ-73: an All-Silica Zeolite with an Unusual Framework Topology

David S. Wragg,[†] Russell Morris,[†] Allen W. Burton,*[,‡] Stacey I. Zones,[‡] Kenneth Ong,[‡] and Greg Lee[‡]

School of Chemistry, The Purdie Building, University of St. Andrews, North Haugh, St. Andrews, Fife, KY16 9ST Scotland, and Chevron Energy Technology Company, 100 Chevron Way, Richmond, California 94802

Received February 26, 2007. Revised Manuscript Received May 7, 2007

This paper reports the synthesis, characterization, and crystallographic studies of the new all-silica zeolite SSZ-73. The framework topology of SSZ-73 is isostructural with the aluminophosphate STA-6 (**SAS**). SSZ-73 is prepared from fluoride-containing gels using 3-ethyl-1,3,8,8-tetramethyl-3-azoniabicyclo-[3.2.1]octane cation as a structure-directing agent. SSZ-73 is an all-silica zeolite with a one-dimensional system of eight-ring pores. However, SSZ-73 possesses a remarkably high micropore volume (0.25 cm^3/g) due to the rather large cages in the structure. A single-crystal X-ray diffraction study of the as-made material shows that fluoride resides within the double six-ring cages of the **SAS** framework. Molecular docking studies were performed for the two geometric isomers of the structure-directing agent in the all-silica frameworks of **SAS**, **RTH**, **ITE**, and **STF**. The studies suggest that the isomer with the ethyl group cis to the bridgehead carbon is the likely structure-directing agent for SSZ-73 and that the other isomer may be responsible for the small amounts of **RTH** impurity observed in some preparations of SSZ-73.

Introduction

Zeolites typically find applications in ion exchange, catalysis, and separations.[1] All-silica zeolites have recently attracted attention as low-dielectric-constant materials for interconnection insulation in microprocessors.[2−4] Advantages of all-silica materials in this application include excellent mechanical strength, high hydrophobicity, and good heat conductivity. In contrast, amorphous and mesoporous silicas possess lower mechanical strength, lower heat conductivity, and higher adsorption uptakes of moisture. The affinity of amorphous silicas for water is due to their high concentration of silanol groups. On the other hand, the ideal (crystallographic) structures of all-silica zeolites are highly hydrophobic because the silica structure is a fully connected tetrahedral framework in which four silicon atoms complete the coordination sphere of every silicon atom (with the exception of the external surfaces of the zeolite crystal, which terminate in silanol groups). As we will later discuss, all-silica zeolites prepared in hydroxide medium necessarily possess negatively charged siloxy/silanol nests that compensate the charge of the organocation occluded within the zeolite structure.[5] However, zeolites prepared in fluoride media generally possess fewer internal silanol defects than zeolites made in hydroxide media. A possible obstacle in the application of zeolites derived from fluoride media is that their crystals tend to be very large. A disadvantage of large crystals is that they give zeolite films with a large surface roughness. Indeed, the dimensions of crystals from fluoride-mediated syntheses are often larger than the typical thickness (<1 micron) of the dielectric film. Nonetheless, the synthesis of zeolites from concentrated fluoride media is a relatively immature science; we anticipate that further studies on the mechanisms of nucleation and crystallization will improve the ability of the zeolite community to control crystallite size in fluoride-mediated syntheses.

Yushan Yan and co-workers have recently discussed that one way to decrease the dielectric constant of a zeolite film is to use an all-silica zeolite with a larger microporosity. They also speculate that small pore sizes are beneficial because they reduce, eliminate, or retard the adsorption of contaminants like water. The ideal zeolite for this application is therefore one with high micropore volume and small (eight-ring) pores that preferably are one-dimensional. One zeotype framework that meets these criteria is the SAS structure. However, until now this structure could only be prepared as a metalloaluminophosphate.

Certain zeotype frameworks that at one time were observed exclusively in aluminophosphate chemistries have recently been discovered in high- or all-silica compositions by use of an appropriate organic structure-directing agent (SDA) molecule. With few exceptions,[6] aluminophosphate zeotypes

* Corresponding author. E-mail: buaw@chevron.com. Phone: 510-242-1810. Fax: 510-242-1792

[†] University of St. Andrews.

[‡] Chevron Energy Technology Company.

(1) Davis, M. E. *Nature* **2002**, *417*, 813−821.
(2) Li, Z.; Li, S.; Luo, H.; Yan, Y. *Adv. Funct. Mater.* **2004**, *14*, 1019.
(3) Li, Z.; Lew, C. M.; Li, S.; Medina, D. I.; Yan, Y. *J. Phys. Chem. B* **2005**, *109*, 8652−8658.
(4) Li, et al. *Angew. Chem., Int. Ed.* **2006**, *45*, 6329−6332.
(5) Koller, H.; Lobo, R. F.; Burkett, S. L.; Davis, M. E. *J. Phys. Chem.* **1995**, *99* (33), 12588−12596.
(6) Afeworki, M.; Dorset, D. L.; Kennedy, G. J.; Strohmaier, K. G. *Stud. Surf. Sci. Catal.* **2004**, *154*, 1274−1281.

10.1021/cm0705284 CCC: $37.00
Published on Web 07/03/2007

Figure 1. Eighteen-ring cage of **MSO** with the occluded carbon atoms (gray) and oxygen atoms (red) of the 18-crown-6 ether molecule.

are usually comprised only of even-numbered rings (i.e., an even number of tetrahedral atoms in the ring) because odd-numbered rings necessitate neighboring tetrahedral T^{III} or T^{V} atoms, a condition that is energetically unfavorable (Lowenstein's rule) because of the juxtaposition of neighboring charges with the same sign. In highly siliceous zeolites, on the other hand, odd-numbered rings frequently comprise a large portion of the rings within a given framework, and exclusively even-ringed structures are relatively uncommon. At the time of its discovery, SSZ-24 was considered unique because it is an all-silica zeolite that possesses exclusively even-numbered rings.[7] The framework of SSZ-24 is isostructural with ALPO-5 (**AFI**), a phase frequently observed in aluminophosphate compositions. SSZ-39, which is isostructural with ALPO-18 (**AEI**),[8] has been prepared using several SDA molecules.[9] SSZ-55 was discovered by Elomari using an SDA derived from a nitrile compound.[10] This zeolite is isostructural with MAPO-36[11] (**ATS**), a magnesioaluminophosphate. It is interesting to note that these aluminophosphates are prepared with SDA molecules that are very distinct from the ones used to prepare their aluminosilicate analogues. For example, the only reported SDA molecule for SSZ-55 is ([(1-(3-fluorophenyl)-cyclopentyl)methyl] trimethylammonium, whereas MAPO-36 uses tri-*n*-propylamine[12] as an SDA. The latter SDA is efficient for making ZSM-5 (**MFI**) in aluminosilicate gels. An exception to this observation includes zeotype materials that have the **MSO** framework topology. Both the aluminosilicate[13] (1,4,7,10,-13,16-hexaoxacyclooctadecane) and the aluminophosphate[14,15] (1,7,10,16-tetraoxa-4,13-diazacyclooctadecane) materials are prepared with 18-crown-6 molecules. Figure 1 demonstrates the match in the size and the shape of these molecules with the large cages of the **MSO** structure.

The metalloaluminophosphate STA-6 (**SAS**) was first prepared by Wright et al. using the azamacrocyle tetramethylcyclam (tmtact) as an SDA in the presence of magnesium.[16,17] Figure 2 shows a framework model of the large cage in this peculiar structure. Note the large cages, which occlude the tmtact-cation complex. Later, the same group discovered[18] that isostructural materials could be prepared with this SDA molecule from aluminophosphate gels using a combination of nickel and magnesium cations, nickel and zinc cations, or rhodium and zinc cations. A structural analysis of the nickel magnesioaluminophosphate indicates that the tmtact preferentially binds the nickel cations.

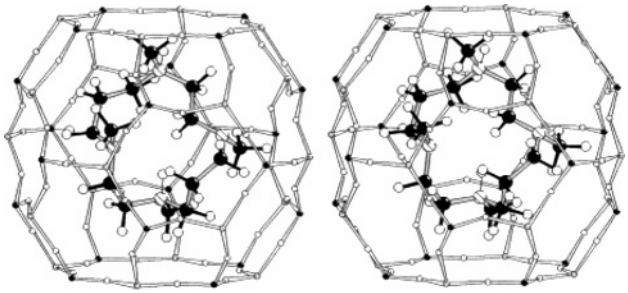

Figure 2. Energy-optimized configuration of the diprotonated 1,4,8,11-tetramethyl-1,4,8,11-tetraazacyclotetradecane within the large cages of STA-6 (from ref 17).

Traditionally, zeolites syntheses have used hydroxide sources to mineralize the silica. However, in the past decade, synthesis in fluoride media has presented a new avenue for the discovery of novel molecular sieves. Flanigen first used fluoride-mediated gels to prepare all-silica **MFI** during the late 1970s,[19] and Guth and Kessler later demonstrated that fluoride could be used as a mineralizing agent to synthesize both zeolites and aluminophosphates from gels with pH values between 6 and 8.[20−22] The zeolite products from their studies often possessed unusually large crystals with few lattice defects. The products from these syntheses are therefore more ideal for crystallographic studies than the micrometer- and submicrometer-sized crystals that are typically obtained in hydroxide-mediated syntheses.

During the mid 1990s, Camblor and Corma began performing fluoride-mediated experiments in highly concentrated gel systems.[23−27] In contrast to most hydroxide-

(7) Bialek, R.; Meier, W. M.; Davis, M.; Annen, M. J. *Zeolites* **1991**, *11*(5), 438−442.
(8) Simmen, A.; McCusker, L. B.; Baerlocher, Ch.; Meier, W. M. *Zeolites* **1991**, *11*, 654−661.
(9) Wagner, P.; Nakagawa, Y.; Lee, G. S.; Davis, M. E.; Elomari, S.; Medrud, R. C.; Zones, S. I. *J. Am. Chem. Soc.* **2000**, *122*(2), 263−273.
(10) Elomari, S.; Zones, S. I. *Proceedings of the 13th International Zeolite Conference*, Mont Pellier, France; Studies in Surface Science and Catalysis; Elsevier: New York, 2001.
(11) Smith, J. V.; Pluth, J. J.; Andries, K. J. *Zeolites* **1993**, *13*, 166−169.
(12) Machado, M. da S.; Cardoso, D.; Perez-Pariente, J.; Sastre, E. *Chem. Mater.* **1999**, *11*(11), 3238−3244.
(13) (a) Shantz D.; Burton A.; Lobo R. *Microporous Mesoporous Mater.* **1999**, *31*, 61−73. (b) Valyosik E.: U.S. Patent 5670131, 1997.
(14) Paillaud, J.; Caullet, P.; Schreyeck, L.; Marler, B. *Microporous Mesoporous Mater.* **2001**, *42*, 177− 89.
(15) Garcia R.; Philip E.; Slawin A.; Wright P.; Cox P. *Proceedings of the 13th International Zeolite Conference*, MontPellier, France; Studies in Surface Science and Catalysis; Elsevier: New York, 2001.
(16) Wright, P. A.; Maple, M. J.; Slawin, A. M. Z.; Patinec, V.; Aitken, R. A.; Welsh, S.; Cox, P. A. *J. Chem. Soc., Dalton Trans.* **2000**, *8*, 1243.
(17) Patinec, V.; Wright, P. A.; Lightfoot, P.; Aitken, R. A.; Cox, P. A. *J. Chem. Soc., Dalton Trans.* **1999**, 3909−3911.
(18) Garcia, R.; Philp, E. F.; Slawin, A. M. Z.; Cox, P. A.; Wright, P. A. *Top. Catal.* **2003**, *24* (1−4), 115−124.
(19) Flanigen E.; Patton R.: US Patent 4 073 865, 1978.
(20) Guth, J.; Kessler, H.; Caullet, P.; Hazm, J.; Merrouche, A.; Patarin, J. *Proceedings of the 9th International Zeolite Conference*; von Ballmoos, R., Higgins, J., Treacy, M., Eds.; Butterworth-Heinemann: London, 1993; p 215.
(21) Kessler, H.; Patarin, J.; Schott-Darie, C. In *Advanced Zeolite Science and Applications*; Jansen, J., Stoecker, M., Karge, H., Weitkamp, J., Eds.: Elsevier: Amsterdam, 1994; pp 75−113.
(22) Guth, J. L.; Kessler, H.; Wey, R. *New Developments in Zeolite Science and Technology; Proceedings of the 7th International Zeolite Conference*, Tokyo, 1986; Murakami, Y., Ijima, A., Ward, J. W., Eds.; Kodansha Ltd.: Tokyo and Elsevier: Amsterdam; pp 121−128.
(23) Barrett, P.; Camblor, M.; Corma, A.; Jones, R.; Villaescusa, L. *J. Phys. Chem. B* **1998**, *102* (21), 4147.
(24) Camblor, M.; Barrett, P.; Diaz-Cabanas, M.; Villaescusa, L.; Puche, M.; Boix, T.; Perez, E.; Koller, H. *Microporous Mesoporous Mater.* **2001**, *48*, 11−22.
(25) Camblor, M.; Corma, A.; Valencia, S. *Chem. Commun.* **1996**, *20*, 2365.
(26) Villaescusa, L.; Barrett, P.; Camblor, M. *Angew. Chem., Int. Ed.* **1999**, *38*, 1997.

mediated syntheses that are carried out with H_2O/SiO_2 between 20 and 60, the H_2O/SiO_2 ratio in these systems was usually between 3 and 15. A large quantity of SDA is often used in these systems (HF, SDA $OH/SiO_2 = 0.5$), and the near-neutral pH is much lower than what is typically encountered in hydroxide-mediated syntheses. This method has succeeded in preparing all-silica versions of highly open framework zeolites that were previously prepared only as borosilicates or aluminosilicates in hydroxide media. One of the first notable examples was an all-silica CHA material prepared with the *N*,*N*,*N*-trimethyladamantammonium cation.[28] Prior to this report, this SDA had been used to prepare zeolite SSZ-13 (**CHA**) only as a highly aluminous ($Si/Al \approx 10-40$) zeolite. Not only has the fluoride route produced open framework zeolites that are often unattainable in the absence of trivalent heteroatoms but it has also yielded a number of all-silica zeolites with new frameworks such as ITQ-7 (**ISV**),[29] ITQ-12 (**ITW**),[30] ITQ-13 (**ITH**),[31] ITQ-27 (**IWV**),[32] ITQ-28,[33] and ITQ-32 (**IHW**).[34]

In these all-silica products, the charge of the occluded SDA cation is counterbalanced by a fluoride anion. Crystallographic[35−42] and solid-state NMR[43−45] studies indicate that fluoride prefers to reside in small cage units, where it may covalently bond with silicon to form pentacoordinated $SiO_{4/2}F^-$. Figure 3 shows the position of fluoride within the double six-ring cages of the all-silica **CHA** structure. An exception to the tendency of fluoride to covalently bond with silicon in zeolite structures occurs when fluoride resides within double four-ring units. In these cases. the fluoride resides at the center of the cage approximately 2.6 Å from the nearest silicon atoms.

Figure 3. Position of the fluoride anion within the double six-ring of **CHA**. For clarity, only one of the 12 symmetry-related positions has been shown with the small cage.

Camblor observed an interesting trend in phase selectivity as the concentration of the gel is changed in fluoride systems.[28] With a particular SDA molecule, products with lower framework density (FD) crystallized as the gel became less dilute. This trend is analogous to what we generally observe in hydroxide systems when the concentration of trivalent heteroatoms (boron, aluminum, or gallium) is increased.[46] A possible explanation for this trend is that high concentrations of fluoride probably favor the formation of small rings or cage units that often comprise open framework materials. Brunner and Meier have reasoned that frameworks with a large proportion of three- or four-ring units are likely to possess low framework density.[47] It could also be reasoned that a higher concentration of negatively charged fluorosilicate species (either at the crystallization or nucleation stages) requires a higher concentration of SDA cations to be associated with the silica. A competition between water and silicate species for the fluoride anion also probably affects the local fluoride concentration within the silicate nuclei. For these reasons, a more open framework may result, because there is more space filling by the SDA molecule.

Recently, we have examined the phase selectivity of many of our SDA molecules in fluoride systems.[48,46,49] The trends that we observe are consistent with those observed in Camblor's early studies. Figure 4 shows the preparation of a polycyclic quaternary ammonium molecule we investigated in ref 49. We will refer to this molecule as B80. At a H_2O/SiO_2 ratio of 7.0, **MWW** is the product with this molecule, and at the high dilution end (14), only an amorphous product is observed. However, at the most concentrated conditions, we observed a new phase that we have designated SSZ-73. Here, we report the synthesis and characterization of this novel material.

Experimental Section

Analytical Methods. Preliminary powder X-ray diffraction (XRD) patterns were recorded on a Siemens D-500 instrument. Scanning electron micrographs (SEM) were recorded on a Hitachi S-570 instrument. Micropore volume was determined from physisorption experiments using nitrogen as an adsorbate. The micropore volume was calculated from a t-plot analysis of the data for the nitrogen isotherm.[50] A calcined sample for detailed structural

(27) Diaz-Cabanas, M.; Barrett, P.; Camblor, M. *Chem. Commun.* **1998**, *17*, 1881.
(28) Camblor, M.; Villaescusa, L.; Diaz-Cabanas, M. *Top. Catal.* **1999**, *587* 9(1−2), 59−76.
(29) Villaescusa, L.; Barrett, P.; Camblor, M. *Angew. Chem., Int. Ed.* **1999**, *38*(13−14), 1997−2000.
(30) Barrett, P.; Boix, T.; Puche, M.; Olson, D.; Jordan, E.; Koller, H.; Camblor, M. *Chem. Commun.* **2003**, *17*, 2114- 2115.
(31) Corma, A.; Puche, M.; Rey, F.; Sankar, G.; Teat, S. *Angew. Chem., Int. Ed.* **2003**, *42*(10), 1156−1159.
(32) Dorset, D. L.; Kennedy, G. J.; Strohmaier, K. G.; Diaz-Cabanas, M. J.; Rey, F.; Corma, A. *J. Am. Chem. Soc.* **2006**, *128* (27), 8862−8867.
(33) Corma, A.; Sabater, M.; Valencia, S. (Zeolita ITQ-28) WO2005030646, 2005.
(34) Cantin, A.; Corma, A.; Leiva, S.; Rey, F.; Rius, J.; Valencia, S. *J. Am. Chem. Soc.* **2005**, *127*, 11560−11561.
(35) Bull, I.; Villaescusa, L.; Teat, S.; Camblor, M.; Wright, P.; Lightfoot, P.; Morris, R. *J. Am. Chem. Soc.* **2000**, *122* (29), 7128.
(36) Villaescusa, L.; Wheatley, P.; Bull, I.; Lightfoot, P.; Morris, R. *J. Am. Chem. Soc.* **2001**, *123*(36), 8797−8805.
(37) Burton, A.; Darton, R. J.; Davis, M. E.; Hwang, S.-J.; Morris, R. E.; Ogino, I.; Zones, S. I. *J. Phys. Chem. B* **2006**, *110* (11), 5273−5278.
(38) Camblor, M.; Diaz-Cabanas, M.; Perez-Pariente, J.; Teat, S.; Clegg, W.; Shannon, I.; Lightfoot, P.; Wright, P.; Morris, R. *Angew. Chem., Int. Ed.* **1998**, *37* (15), 2122−26.
(39) Van de Goor, G.; Freyhardt, C.; Behrens, P. *Anorg. Allg. Chem.* **1995**, *621*, 311.
(40) Caullet, P.; Guth, J.; Hazm, J.; Lamblin, J.; Gies, H. *Eur. J. Solid State Inorg. Chem.* **1991**, *28*, 345.
(41) Villaescusa, L.; Bull, I.; Wheatley, P.; Lightfoot, P.; Morris, R. *J. Mater. Chem.* **2003**, *13* (8), 1978−1982.
(42) Corma, A.; Puche, M.; Rey, F.; Sankar, G.; Teat, S. *Angew. Chem., Int. Ed.* **2003**, *42* (10), 1156−1159.
(43) Camblor, M.; Diaz-Cabanas, M.; Cox, P.; Shannon, I.; Wright, P.; Morris, R. *Chem. Mater.* **1999**, *11* (10), 2878−2885.
(44) Fyfe, C.; Brouwer, D.; Lewis, A.; Villaescusa, L.; Morris, R. *J. Am. Chem. Soc.* **2002**, *124* (26), 7770−7778.
(45) Koller, H.; Wolker, A.; Villaescusa, L.; Diaz-Cabanas, M.; Valencia, S.; Camblor, M. *J. Am. Chem. Soc.* **1999**, *121* (14), 3368.
(46) Zones, S.; Hwang, S.; Elomari, S.; Ogino, I.; Davis, M.; Burton, A. *C. R. Chim.* **2005**, *8* (3−4), 267−82.
(47) Brunner, G. O.; Meier, W. M. *Nature* **1989**, *337*, 146−147.
(48) Zones, S. I.; Darton, R. J.; Morris, R.; Hwang, S.-J. *J. Phys. Chem. B* **2005**; *109* (1), 652−661.
(49) Zones, S. I.; Burton, A. W.; Lee, G. S.; Olmstead, M. M. *J. Am. Chem. Soc.* **2007**, *129*, accepted.
(50) Lippens, B. C.; Boer, J. H. D. *J. Catal.* **1965**, *4*, 319.

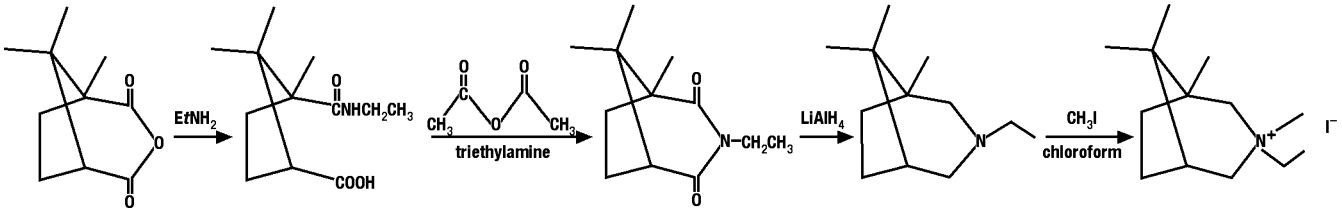

Figure 4. Reaction steps to prepare the SDA for SSZ-73.

analysis was examined at Beamline X16C at Brookhaven National Laboratory. Data were collected at ambient temperature from 6 to 65° 2θ with a step size of 0.005° 2θ using a wavelength of 1.19958 Å. Data were collected for 2 s/step from 6 to 37° 2θ and for 4 s/step from 37 to 60° 2θ. The X16C sample was packed and sealed in a 1.0 mm diameter glass capillary. The starting model for the Rietveld structure refinement was generated from an energy-optimized model of an all-silica framework in space group *I*4/*mmm*. The organic content of the as-made zeolite was measured from C/H/N combustion analyses.

Single-crystal X-ray diffraction data for three samples of as made SSZ-73 were collected on Station 9.8 at the Synchrotron Radiation Source (SRS), Daresbury Laboratories, Cheshire, UK. The structure was solved using standard direct methods and refined using the least-squares minimization techniques against F^2. Unfortunately, all three refinements are of relatively poor quality (R1 > 20%) but were of sufficient quality to allow location of all the framework atoms in the structure, including the fluoride ions, from difference Fourier electron density maps. The high symmetry of the structure and the consequent disorder that this imposes on the organic structure-directing agent renders it impossible to refine from the diffraction data. Use of the Squeeze routine from the Platon suite of programs[51] to remove the scattering from the pores of the zeolite leads to improved refinements (R1 = 0.15 for the best of the three refinements). The final refined Si−F distance is 2.04(8) Å (which is in the expected range for such structures) and the refined occupancy is 0.11(2). However, in such low-quality refinements, the occupancy in particular should be treated as an approximate result.

Energy minimizations of the SDA within different frameworks were performed with the Cerius2[52] software using a combination of the Burchart[53] and Universal forcefields[54] to evaluate the van der Waals interactions of the SDA molecule with the zeolite framework and the intramolecular interactions of the SDA. To simplify the calculations, we model each zeolite structure as an all-silica framework, and we neglect coulombic interactions between the SDA molecule and the fluoride anions. The calculations are performed on periodic structures using a single unit cell. No supercells are required for most of the cage-based frameworks considered, because the molecular dimensions do not exceed the unit-cell dimensions and there are negligible interactions between SDA in neighboring cage structures (i.e., each cage effectively isolates its occluded SDA molecule). During the energy-minimization process, the atoms of the zeolite framework are held fixed. To find the true global minimum for each SDA molecule, we exhaustively sample multiple initial configurations (and molecular conformations as appropriate). The stabilization we report is the difference between the energy of the molecule occluded in the framework and the minimum energy of the free (gas phase) molecule. Because we are primarily concerned with how the silica phase is stabilized, we normalize the absolute stabilization energy (per mole of SDA) by dividing by the appropriate number of T atoms in the unit cell.

The SDA (3-ethyl-1,3,8,8-tetramethyl-3-azoniabicyclo[3.2.1]-octane cation) was prepared[55] according to a procedure (Figure 4) similar to that described by Nakagawa.[56] In summary, the molecule is prepared by reaction of a parent anhydride (camphoric anhydride) with ethylamine to form a carboxylic acid/amide intermediate. This is then reacted with acetic anhydride to form a ring-closed imide. This imide is next reduced to a tertiary amine with lithium aluminum anhydride. The amine is subsequently alkylated with methyl iodide to form a quaternary ammonium molecule.

In the first step, a 5 L flask was equipped with a mechanical stirrer and reflux condenser. The flask was charged with 107.0 g of camphoric anhydride, and 1400 mL of ethylamine was added. Some gas was evolved with a slight exotherm. Next, 14.44 g of 4-dimethylaminopyridine (caution, toxic compound) was added, and the mixture was stirred at room temperature for 2 h and then refluxed overnight. The reaction was then cooled to room temperature, and the pH was adjusted to below 2 with the addition of concentrated HCl. At this point, a sticky solid precipitated from solution. The mixture was extracted three times with 500 mL portions of ethyl acetate. The ethyl acetate extracts were then dried over anhydrous magnesium sulfate and subsequently rotoevaporated to give 130.9 g of an off-white solid.

The product from the above step was then mixed with 117.7 g of triethylamine and 580 mL of acetone and heated to reflux; 89.1 g of acetic anhydride was then added dropwise to the mixture over a period of 30 min. The mixture was refluxed with mixing over a course of 3 days. The reaction was allowed to cool to room temperature and the acetone was removed by rotoevaporation. Two hundred milliliters of deionized water was then added to the yellow oil residue, and the pH was adjusted to below 2 with concentrated HCl. The aqueous solution was then extracted three times with 200 mL portions of ethyl acetate. The ethyl acetate extracts were then combined and twice washed with 200 mL portions of 1 N NaOH. The ethyl acetate solution was dried over anhydrous magnesium sulfate and rotoevaporated to yield 117.5 g of a yellow oil.

In the next step, a 5 L flask was equipped with a mechanical stirrer, a reflux condenser, a nitrogen gas inlet/outlet, and an addition funnel. The flask was placed within an ice bath under a nitrogen flow, and 67.2 g of lithium aluminum hydride (LAH) and 1580 mL of ethyl ether were added to the flask. The imide product (117.4 g) from the previous step was then dissolved in 792 mL of anhydrous methylene chloride. The imide solution was then added to the LAH suspension over a 30 min period. The reaction was stirred at room temperature for 3 days; 61.4 mL of water was then

(51) Spek, A. L. *J. Appl. Crystallogr.* **2003**, *36*, 7−13.
(52) *Cerius2*, version 2.1; Molecular Simulations (BioSym): Cambridge, UK, 1997.
(53) de Vos Burchart, E. Studies on Zeolites: Molecular Mechanics, Framework Stability and Crystal Growth. Ph.D. Thesis, Delft University of Technology, Delft, The Netherlands, 1992; Chapter XII, Table 1.
(54) (a) Rappe, A. K.; Casewit, C. J.; Colwell, K. S.; Goddard, W. A., III; Skill, W. M. *J. Am. Chem Soc.* **1992**, *114*, 10024. (b) Castonguay, L. A.; Rappe, A. K. *J. Am. Chem. Soc.* **1992**, *114*, 5832−5834. (c) Rappe, A. K.; Colwell, K. S. *Inorg. Chem.* **1993**, *32*, 3438−3450.
(55) Zones, S. I.; Burton, A. W.; Ong, K., U. S. Patent 7 138 099, 2006.
(56) Nakagawa, Y. U. S. Patent 5 268 161, 1993.

added and methylene chloride was also added to replace the ethyl ether that evaporated during the exotherm. Then, 61.4 g of 15% NaOH was slowly added, followed by 184.6 g of additional water. After the solids in the reaction mixture turned from gray to white, the solids were removed by filtration and washed with methylene chloride. Four hundred milliliters of water was then added to the filtrate and the pH was adjusted to below 2 with concentrated HCl. The aqueous and organic phases were then separated; 200 mL of water was added to the organic phase, the pH was again adjusted to below 2, and the phases were again separated. The aqueous phases were combined and the pH was then adjusted to above 12 with 50% NaOH. This solution was then saturated with sodium chloride and extracted four times with 250 mL portions of ethyl acetate. The combined ethyl acetate extracts were then dried over anhydrous magnesium sulfate and the amine product was recovered by rotoevaporation (65.9 g).

For the final step, a 500 mL flask was equipped with a magnetic stirrer and addition funnel. The flask was charged with 32.92 g of amine (0.18 mol) and 180 mL of chloroform. Iodomethane (52.06 g, 0.36 mol) was then added dropwise to the solution over a 5 min period. The reaction was stirred at room temperature for 4 days. The product was precipitated from solution with ethyl ether and then recovered by filtration. The yellow solids (52.0 g) were then recrystallized from hot acetone and a minimal amount of methanol.

The quaternary ammonium compound was then anion-exchanged into its hydroxide form by dissolving the salt in water and adding a 2-fold excess of Bio-Rad AG 1-X8 ion-exchange resin (20−50 mesh, hydroxide form). After removal of the resin, the hydroxide concentration of the aqueous solution was determined by titration with a standard solution 0.1 M HCl using phenolphthalein as an indicator.

Zeolite Synthesis. SSZ-73 was prepared in fluoride media using the 3-ethyl-1,3,8,8-tetramethyl-3-azoniabicyclo[3.2.1]octane cation as an SDA. In a typical experiment, 1.35 g of tetraethylorthosilicate (TEOS) and 3.25 mmol of hydroxide (from an aqueous solution of the SDA in its hydroxide form) were added together in a 23 mL Teflon liner. The ethanol (formed from the hydrolysis of the TEOS) and water were allowed to evaporate within a vented hood with flowing air over the course of 3−7 days. The extent of evaporation was monitored by measuring the weight of the liner and its contents. Then, 0.13 g of 50% HF and the appropriate amount of water were added and mixed to create a uniform gel in which the H_2O/SiO_2 ratio was 3−3.5. The liner was then capped and placed within a Parr Steel autoclave reactor. The autoclave was then fixed in a rotating spit within an oven heated at 150 or 170 °C. The progress of the crystallization was monitored by periodically removing the autoclave, allowing the autoclave to cool, and then removing a small amount of sample for SEM analysis. Typically, the synthesis of SSZ-73 required 10−15 days at 150 °C. The product from the synthesis was washed with at least 150 mL of deionized water. A portion of the sample was calcined by heating in a flow of 2% air in nitrogen to 595 °C at 1 °C/min and holding the temperature at 595 °C for 6 h.

Results and Discussion

Preliminary Characterization. Figure 5a shows a powder XRD pattern of an initial preparation of SSZ-73, and Figure 6a shows the SEM of this same product. The planklike crystals were typically about 2−4 μm thick and 10−40 μm long. At first we did not recognize the phases in the powder XRD pattern. A search/match of the ICDD database with

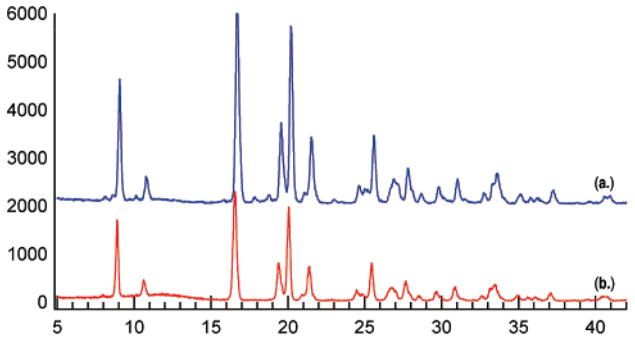

Figure 5. Powder XRD (Cu Kα) patterns of (a) an early preparation of SSZ-73 and (b) a later preparation of SSZ-73 with fewer impurities.

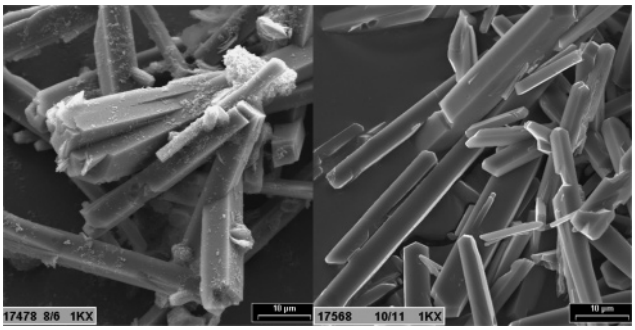

Figure 6. SEM images of (a) an early preparation of SSZ-73 and (b) a later preparation of SSZ-73 with fewer impurities.

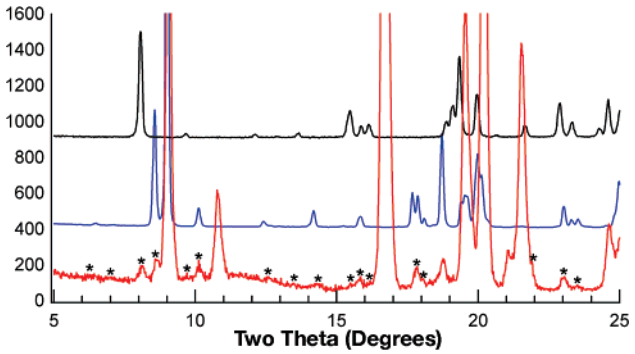

Figure 7. Powder XRD pattern of initial sample of SSZ-73 (bottom), with small impurities indicated by asterisks. The middle pattern is a scaled-down experimental pattern for an all-silica **RTH** material prepared in fluoride medium, and the top pattern is a scaled-down reference pattern for **STF**. Note that the symmetry of the **RTH** material is lower than those prepared in non-fluoride medium and that the low-angle peaks between 5.5 and 7.5° are absent in the *C*2/*m* symmetry of **RTH**.

JADE[57] revealed a close match between STA-6 (**SAS**) and the major peaks in this pattern. These matched peaks could be indexed in a tetragonal cell with $a = 14.09$ and $c = 10.17$ Å. The close resemblance of the unit cell and peak intensities suggested that the major phase was an all-silica zeolite with the **SAS** topology. Analysis of the smaller, unidentified peaks in the pattern (marked with asterisks in Figure 7) revealed that the remaining phases were likely a mixture of **STF** (major peak near 8° 2θ) and **RTH** (major peak at 8.5 ° 2θ). **RTH** prepared in fluoride media has a lower symmetry than the material prepared in hydroxide medium. This is most evident by the appearance of two low-angle peaks between 5.5 and 7.5° 2θ. It is interesting to note that neither of these impurity phases is observed as a product for the other synthesis concentrations. Furthermore, in our experiments,

(57) *JADE*; Materials Data: Livermore, CA.

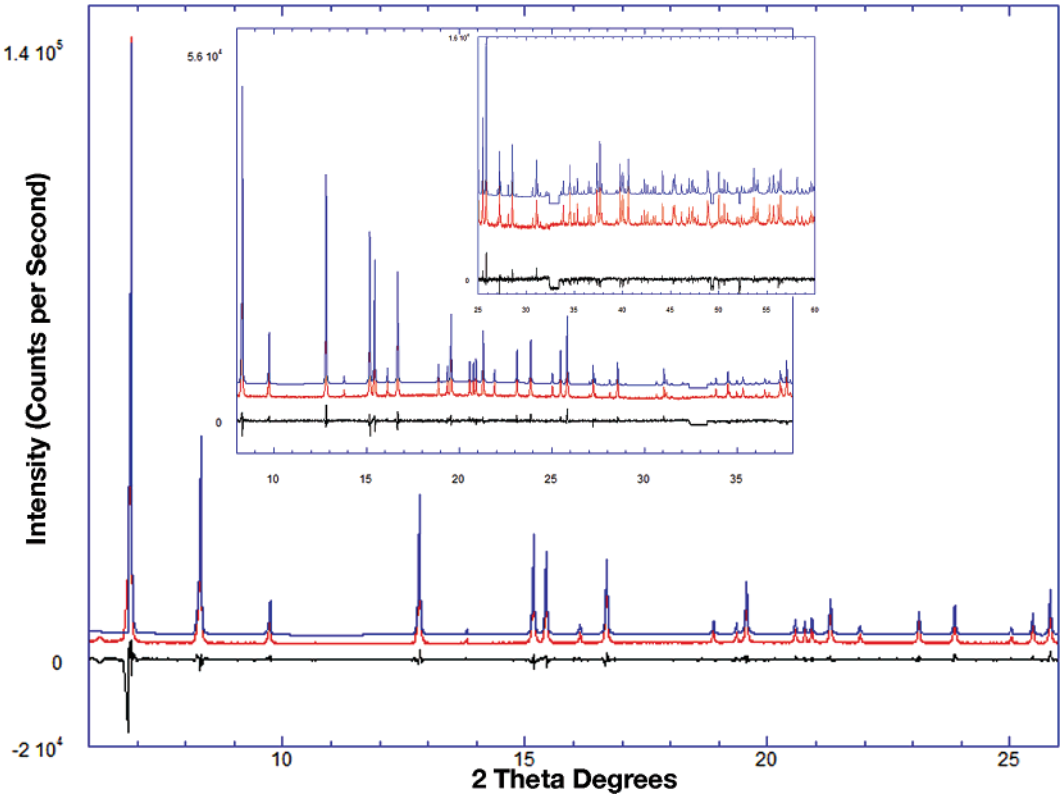

Figure 8. Simulated (top), experimental (middle), and difference (bottom) profiles with Rietveld refinement of a calcined sample of SSZ-73 with λ = 1.19958 Å.

no high-silica zeolite phases were prepared with B80 in hydroxide media. However, if the *N*-ethyl group is replaced with a methyl group, then the SDA molecule (B74) is very selective for **STF** for H_2O/SiO_2 ratios from 3.5 to 14 (in fluoride media). In hydroxide media, the same molecule can be used to prepare **STF** phases for gels with Si/Al above 20 and SSZ-36 (**ITE**/**RTH** intergrowth) phases[58] for Si/Al of 15. One possibility is that during the course of the synthesis, the SDA for SSZ-73 degrades to form a molecule that directs the crystallization of these impurity phases. For example, elimination of the ethyl group in B80 would yield a molecule that is similar to B74 with the exception of an extra methyl group at the N-position. Another issue we have not discussed is the separate structure-directing effects of the two possible isomers of B80. Note that after the quaternization step to prepare B80, the ethyl group can be located either on the same side or on the opposite side of the ring where the bridging methylene resides. It could be that the less-preferred isomer is responsible for the minor impurities. Future synthesis and separation studies will examine this issue.

The XRD patterns of later preparations (Figure 5b) showed no **RTH** impurity, and only the major peak of **STF** at 8.0 degrees could be observed. The SEM (Figure 6b) also appeared less "fuzzy" than those for the previous sample. In any case, these results have suggested another potential SDA cation for **RTH**. This is interesting because very few SDA molecules are known to make **RTH** (without **ITE** intergrowths) as either an aluminosilicate or pure-silica material. The SDA molecule for SSZ-50 (**RTH**)[59] requires a multistep reaction involving a Michael addition, and RUB-13[60] is prepared with pentamethylpiperidine only in borosilicate systems.

Table 1. Refined Atomic Parameters of Calcined SSZ-73 in Space Group *I*4/*mmm* (No. 139); *a* = 14.1039(1) Å, *c* = 10.1875(1) Å

atom	*x*	*y*	*z*	U_{iso}
Si1	0.2658(2)	0.1098(2)	0	0.005
Si2	0.6090(1)	0.8910(1)	3/4	0.005
O1	0.2386(5)	0	0	0.005
O2	0.3255(2)	0.8623(2)	0.8735(4)	0.005
O3	1/2	0.8739(3)	0.7893(5)	0.005
O4	0.1685(4)	0.8316(4)	0	0.005

Structure of the Calcined Zeolite. To verify the structure of the material, we collected synchrotron powder X-ray diffraction data on a calcined sample of SSZ-73 that possessed a minor amount of **STF** impurity. There is a 2.7% increase in the cell volume after calcination, with the *c* dimension remaining nearly the same. The structure refined smoothly, and no bond or angle restraints were necessary throughout the refinement. Table 1S in the Supporting Information shows the refined bond lengths and bond angles, and Table 2S in the Supporting Information shows a summary of the experimental details and refinement parameters. Figure 8 shows the experimental, simulated, and difference profiles for the powder pattern of SSZ-73. Table 1 shows the refined atomic coordinates of the atoms. The agreement factors were R_p = 8.12% and R_{wp} = 12.24%. There is very good visual agreement between the experi-

(58) Wagner, P.; Nakagawa, Y.; Lee, G. S.; Davis, M. E.; Elomari, S.; Medrud, R. C.; Zones, S. I. *J. Am. Chem. Soc.* **2000**, *122*(2), 263−273.

(59) Lee, G. S.; Zones, S. I. *J. Solid State Chem.* **2002**, *167*, 289−298.

(60) Vortmann, S.; Marler, B.; Gies, H.; Daniels, P. *Microporous Mater.* **1995**, *4*, 111−121.

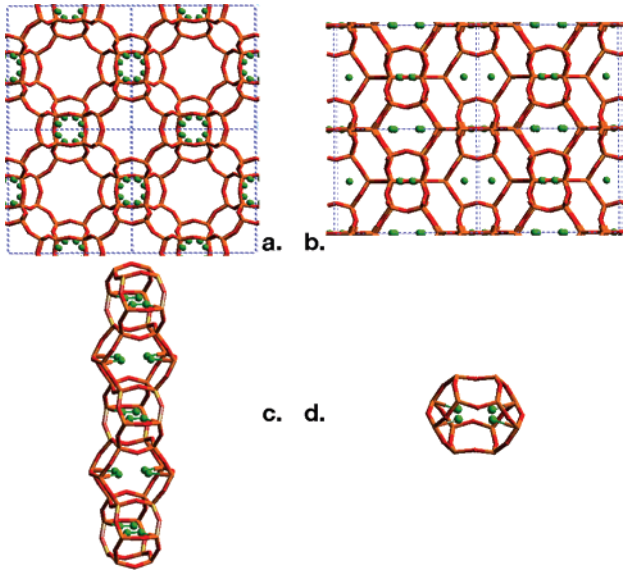

Figure 9. (**a)** Crystallographic model of as-made SSZ-73 with view along the 001 direction (b) Crystallographic model of as-made SSZ-73 with view along the 100 direction. (c) Double six-ring columns in SSZ-73. (d) An isolated double 6-ring cage showing the symmetry-related positions of the fluoride anions.

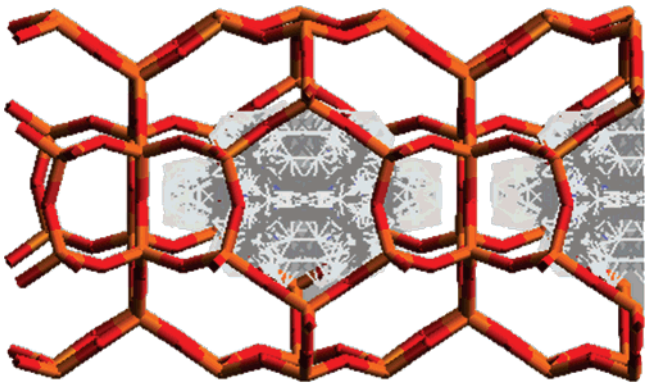

Figure 10. Symmetry-related atomic positions of the energy-optimized configuration of B80 in the **SAS** framework.

Table 2. Refined Atomic Parameters of As-made SSZ-73 in Space Group *I*4/*mmm* (No. 139); $a = 13.9188$ Å, $c = 10.1820$ Å

atom	*x*	*y*	*z*	U_{eq}
Si1	0.2678(4)	0.1109(3)	0.0000	0.0092(12)
Si2	0.3891(4)	0.1109(4)	0.2500	0.0323(19)
O1	0.2377(14)	0.0000	0.0000	0.012(3)
O2	0.5000	0.1266(15)	0.2119(19)	0.037(5)
O3	0.3257(12)	0.1399(10)	0.1289(16)	0.052(5)
O4	0.1692(11)	0.1692(11)	0.0000	0.027(6)
F1	0.400(6)	0.043(6)	0.0000	0.050

mental and simulated patterns. Note that there are a few small regions where the experimental data were not used (e.g., around 33° 2θ); during the latter stages of data collection, there were severe thunderstorms that passed through Long Island, NY. These storms caused the synchrotron beam to "dump" a few times during the course of data collection. Despite corrective adjustments, after these beam dumps, there were small step changes in the background that cannot be modeled well. This was not a problem for our data because these regions contained very few peaks or peaks of minor intensity.

The T-atom density of the calcined SSZ-73 is 15.8 Si/1000 Å^3. Note that this is only slightly lower than the framework density for **RTH** and **ITE**[61] (FD $\approx$ 16.2) materials. In fact, these three structures have similar structural motifs. In each framework, there are columns composed of repeating polyhedral cage units. **RTH** and **ITE** possess the same columns, which are comprised of interlinked 4^45^4 polyhedral units, but the neighboring columns are related by different symmetry elements. In **SAS**, the columns (see Figure 9c) are composed of adjoining double six-ring units that are connected by a common four-ring unit. Within each column, every D6R is rotated 90° (about the column axis) relative to its adjacent D6R neighbors. In the **SAS** framework, each column is related to its neighboring columns by a mirror plane. When four columns are linked together, they create a large cage structure with eight-ring windows.

The measured micropore volume of calcined SSZ-73 is 0.25 cm^3/g. For a one-dimensional eight-ring zeolite, this is an astoundingly large micropore volume. For comparison, the micropore volumes of SSZ-50 (**RTH**)[62] and SSZ-35 (**STF**) are 0.22 and 0.20 cm^3 per gram, respectively. **RTH** possesses a two-dimensional eight-ring pore system and **STF** possesses a one-dimensional 10-ring pore system.

Structure of As-Made Zeolite. For the ideal case of one SDA molecule per large cage, we expect a chemical formula of $C_{13}NH_{24}$·F·16SiO_2. This organic content compares well with the data from CHN combustion analyses: 13.49% C (13.29% expected), 1.27% N (1.19%), and 2.29% H (2.04%). We were interested in examining the location of fluoride within the **SAS** structure. Because all previous studies show that fluoride prefers small cages, anticipating the location of the fluoride anion was reasonably simple because there is a single type of small cage (the D6R) in the structure. However, we also wanted to investigate which T site the fluoride prefers. Recently Pulido[63] et al. have performed computational studies that rationalize and predict the locations of fluoride in a given zeolite prepared with a particular SDA molecule. Their studies indicate that the preferred cage is determined by long-range electrostatic interactions between the SDA cation and the fluoride. The preferred silicon site within the preferred cage is determined by the energetics of the Si−F bond.

Because the SSZ-73 crystals were fairly large, we were able to perform microcrystal diffraction experiments at a synchrotron source. However, despite attempts to collect data with three different crystals, the overall diffraction intensity was not sufficient to allow a meaningful refinement of the atoms in the SDA cation. Table 2 shows the atomic coordinates determined for the framework atoms of the as-made zeolite. We were unable to locate the position of the SDA molecule. This was hampered by the quality of the diffraction data and in part by the high symmetry (*I*/4*mmm*) of the material, which effectively "smears" the scattering intensity of the organic molecule throughout much of the

(61) Camblor, M. A.; Corma, A.; Lightfoot, P.; Villaescusa, L. A.; Wright, P. A. *Angew. Chem., Int. Ed.* **1997**, *36*, 2659−2661.
(62) Lee, G. S.; Zones, S. I. U.S. Patent 6 605 267, 2003.
(63) Pulido, A.; Corma, A.; Sastre, G. *J. Phys. Chem. B* **2006**, *110* (47), 23951−23961.

cage. This is demonstrated in Figure 10, which shows the symmetry related locations of the energy-minimized position (vide infra) of the SDA molecule within the **SAS** framework. Furthermore, the possibility of static disorder cannot be dismissed.

Nonetheless, we were able to locate the framework atoms and the fluoride anions. Panels a and b of Figure 9 show the symmetry-related positions of the fluoride anion along 001 and 100 directions. The fluoride−Si1 distance is 2.04 Å, which is somewhat longer than ideal Si−F distances of 1.7−1.9 Å, but consistent with those determined in other crystallographic studies of fluoride-containing zeolites. The location is similar to that observed in the F-CHA structure, where the measured Si−F distance is 2.02 Å.[64] Because there are two large cages per unit cell that accommodate an SDA cation, only 1/8 of the symmetry-related sites may be occupied by a fluoride anion. The refined occupancy of 0.11-(2) is very close to the ideal occupancy of 1/8.

Molecular Modeling. To understand why B80 is effective for making SSZ-73, we performed energy-minimization calculations of this molecule within the **SAS**, **RTH**, **ITE**, and **STF** frameworks. The latter three frameworks were chosen for comparison with **SAS** because they are often made with SDA molecules of similar size and shape. Indeed, even within the synthesis of SSZ-73, we observe small impurities of **RTH** and **STF** (vide supra). Because **SAS** is not a frequently observed phase, we speculate that this framework may require more stabilization (from its SDA molecule) to improve its kinetic favorability relative to phases like **ITE**, **RTH**, and **STF**. We were also interested in examining the possibility that the less-preferred geometric isomer of B80 is responsible for at least one of the impurities that we observe. We therefore performed calculations for each isomer. Furthermore, we were curious to know why **RTH** was being made rather than **ITE**. The framework structures are very similar and differ only by a single-symmetry operation. In our previous molecular modeling, we rarely observe much difference in stabilization for molecules within the **ITE** and **RTH** frameworks because their cages are so similar in shape. Figure 11 shows a comparison of the **SAS**, **RTH**, and **ITE** cages.

Table 3 shows the stabilizations (reported on a per T atom basis) of each isomer in the different frameworks. Because each framework possesses 16 T atoms per large cage, these structures provide a good basis of comparison for stabilization whether it is on a per-T-atom basis or on a per-SDA basis. The relative order of framework density (FD, T atom/nm^3) for each of the frameworks is **SAS** (15.7), **RTH** (16.1), **ITE** (16.3), and **STF** (17.3). If the expected correlation holds for framework energy versus density,[65,66] then we anticipate that the **SAS** framework possesses higher energy than the other frameworks in this group. For both isomers, the **SAS** framework possesses the best stabilization and **RTH** has the next-closest stabilization. However, the difference is greater

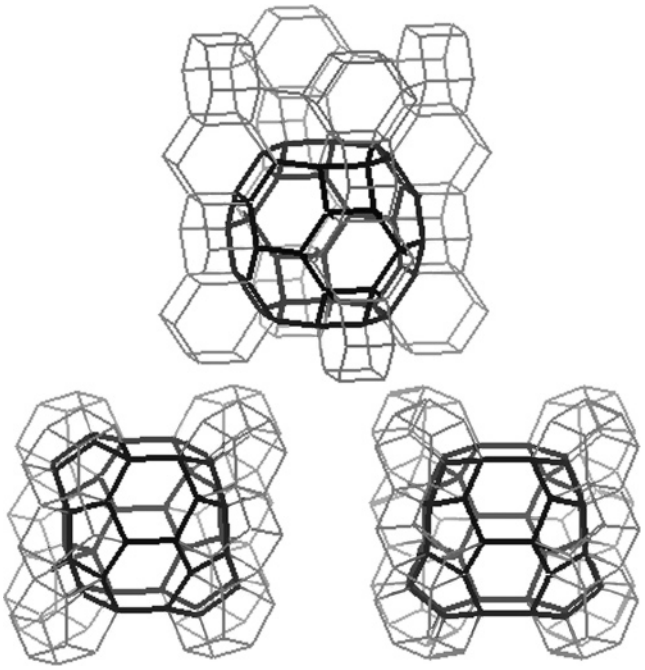

Figure 11. Cages with surrounding columnar units found in the frameworks of (top) **SAS**, (left, bottom) **RTH**, and (right, bottom) **ITE**. The models have been constructed on the same scale to illustrate the relative dimensions of the cages in each structure. Note that the columns in **SAS** are composed of $6^2 4^6$ polyhedral cages, and the columns in **RTH** and **ITE** are composed of $4^4 5^4$ polyhedral cages.

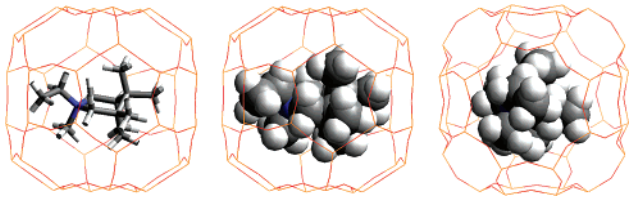

Figure 12. Energy-optimized configuration of B80 isomer B in **SAS**. The image on the right has been rotated by 90° about a vertical axis through the middle of the cage.

Table 3. Energy Minima (kJ mol^{-1} T^{-1}) of the Optimized Configuration of Isomers of B80 in the SAS, RTH, ITE, and STF Frameworks

Molecule	SAS	RTH	ITE	STF
A. 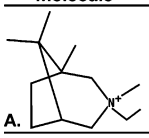	-12.3	-12.0	-11.1	-10.1
B. 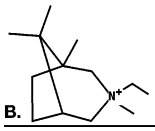	-12.5	-11.8	-11.2	-10.6

for the isomer with the ethyl group cis to the dimethyl bridge. Figure 12 shows different views of the energy-optimized configuration of this molecule in the **SAS** structure. In this case, **SAS** is −0.7 kJ/mol T atom more stabilized than **RTH**; if the ethyl is trans, the difference is only −0.3 kJ/mol T atom. From these considerations alone, we believe that the cis isomer is the likely SDA molecule for SSZ-73. The calculations show that **RTH** is preferred over **ITE** for both isomers (−0.6 and −0.9 kJ/mol T atom). These differences are too small to allow a reasonable assessment of which isomer may be responsible for the **RTH**. If **RTH** is indeed

(64) Villaescusa, L. A.; Bull, I.; Wheatley, P. S.; Lightfoot, P.; Morris, R. E. *J. Mater. Chem.* **2003**, *13*, 1978−1982.
(65) Piccione, P. M.; Laberty, C.; Yang, S.; Camblor, M. A.; Navrotsky, A.; Davis, M. E. *J. Phys. Chem. B* **2000**, *104* (43), 10001−10011.
(66) Henson, N. J.; Cheetham, A. K.; Gale, J. D. *Chem. Mater.* **1994**, *6*(10), 1647−1650.

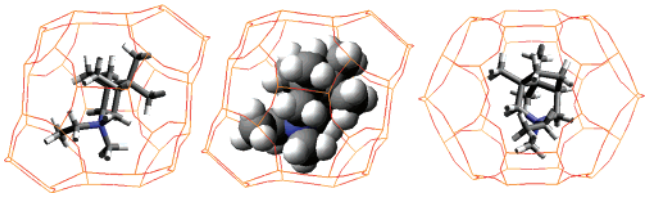

Figure 13. Energy-optimized configuration of the Isomer A of B80 in **RTH**. The image on the right has been rotated by 90° about a vertical axis through the middle of the cage.

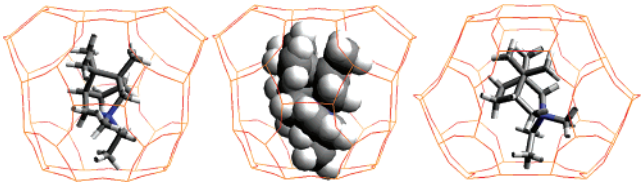

Figure 14. Energy-optimized configuration of the isomer A of B80 in **ITE**. The image on the right has been rotated by 90° about a vertical axis through the middle of the cage.

formed from a less-preferred isomer, then the conclusion would be that trans isomer is responsible for the formation. Figures 13 and 14 show different views of the energy-optimized configuration of isomer A of B80 within the **RTH** and **ITE** cages, respectively. It is apparent that the shape of the molecule conforms well to the shape of the **RTH** cage. In particular, the "flippers" of the cage allow extra room for the methyl and ethyl groups at opposite ends of the molecule. In contrast, the "flippers" of the **ITE** cage are positioned at the same end of the cage and therefore the molecule cannot adopt a similar configuration. This configuration is about 0.9 kJ/mol SiO_2 less stable than the one observed for the **RTH** cage.

The above assessments are highly speculative. However, we will soon address these predictions by carrying out separations of the putative isomers. With the pure isomers, we can then examine how well the calculations correlate with experimental results. In this example, not only have we rationalized experimental results but we have also used molecular modeling as a predictive tool.

Conclusions

For the first time, a siliceous version of the **SAS** structure has been synthesized. This has been accomplished by using a polycyclic SDA molecule in fluoride media. The **SAS** framework topology has been confirmed both by Rietveld refinement of synchrotron powder diffraction data of the calcined material and by refinement of single-crystal data of the as-made structure. The fluoride in the as-made material is located within the double six-ring units of the **SAS** framework. Molecular modeling of the SDA molecule within the **SAS** framework shows an excellent fit compared to fits within frameworks of other phases (**RTH**, **ITE**, and **STF**) expected to compete in this chemistry with similar structure-directing agents. From the molecular modeling, we speculate that the small impurities with the SSZ-73 product may be due to a less-preferred geometric isomer of the B80 molecule.

Acknowledgment. We thank Tom Rea for collection of the SEM data. This work was supported by the Chevron Energy Technology Company. We are grateful to G. L. Scheuerman and C. R. Wilson for support of the new materials research program at Chevron. We also acknowledge the assistance of Jae-Hyuk Her and Peter Stephens in the collection of the synchrotron diffraction data at X16C. Research was carried out in part at the National Synchrotron Light Source, Brookhaven National Laboratory, which is supported by the U.S. Department of Energy, Division of Materials Sciences and Division of Chemical Sciences.

Supporting Information Available: Tables 1S and 2S. This material is available free of charge via the Internet at http://pubs.acs.org.

CM0705284